Remote Sensing of Environment 114 (2010) 2624–2636

Contents lists available at ScienceDirect

Remote Sensing of Environment

journal homepage: www.elsevier.com/locate/rse

Landslide susceptibility mapping using downscaled AMSR-E soil moisture: A case study from Cleveland Corral, California, US

Ram L. Ray [a,*], Jennifer M. Jacobs [b], Michael H. Cosh [c]

[a] Department of Civil and Construction Engineering, San Diego State University, USA
[b] Department of Civil Engineering, University of New Hampshire, 35 Colovos Rd. Durham, NH 03824, USA
[c] USDA ARS, Hydrology and Remote Sensing Lab, Beltsville, MD 20705, USA

ARTICLE INFO

Article history:
Received 3 November 2009
Received in revised form 28 April 2010
Accepted 31 May 2010

Keywords:
AMSR-E
Remote sensing
VIC-3L
Landslide
Soil moisture
Slope stability

ABSTRACT

As soil moisture increases, slope stability decreases. Remotely sensed soil moisture data can provide routine updates of slope conditions necessary for landslide predictions. For regional scale landslide investigations, only remote-sensing methods have the spatial and temporal resolution required to map hazard increases. Here, a dynamic physically-based slope stability model that requires soil moisture is applied using remote-sensing products from multiple Earth observing platforms. The resulting landslide susceptibility maps using the advanced microwave scanning radiometer (AMSR-E) surface soil moisture are compared to those created using variable infiltration capacity (VIC-3L) modeled soil moisture at Cleveland Corral landslide area in California, US. Despite snow cover influences on AMSR-E surface soil moisture estimates, a good relationship between the downscaled AMSR-E's surface soil moisture and the VIC-3L modeled soil moisture is evident. The AMSR-E soil moisture mean (0.17 cm^3/cm^3) and standard deviation (0.02 cm^3/cm^3) are very close to the mean (0.21 cm^3/cm^3) and standard deviation (0.09 cm^3/cm^3) estimated by VIC-3L model. Qualitative results show that the location and extent of landslide prone regions are quite similar. Under the maximum saturation scenario, 0.42% and 0.49% of the study area were highly susceptible using AMSR-E and VIC-3L model soil moisture, respectively.

© 2010 Elsevier Inc. All rights reserved.

1. Introduction

Remote-sensing and spatial analysis tools are widely used in landslide studies including landslide detection, landslide assessment, natural hazard, landslide mapping, and landslide inventories (e.g., Gorsevski et al., 2003; Guzzetti et al., 1999; Pradhan et al., 2006; van Westen, 1994; Varnes, 1984). Remote-sensing data can be used to predict catastrophic events and hazardous areas (Ostir et al., 2003) and they have significant potential for landslide studies (Hong et al., 2007).

Landslide inventory maps can be developed by field surveying. However, surveying is time consuming, expensive and difficult for regional or global scales. On the other hand, landslide inventory maps can be developed using aerial photography (Braddinoni et al., 2003; Oka, 1998; van Westen & Getahun, 2003) as well as remotely sensed data with image analysis technique (Abdallah et al., 2007; Nichol & Wong, 2005). Over the past decade, the Earth Observing System (EOS) platforms have deployed a suite of instruments that monitor land conditions relevant to landslide hazard characterization such as Light Detection and Ranging (LiDAR), Interferometric Synthetic Aperture Radar (InSAR), and Differential SAR Interferometry (DInSAR) data. The predominant use of remotely sensed data is to map landslides after they have occurred using aerial photographs (van Westen & Getahun, 2003), to characterize landslide distributions using aerial photographs (Carrara et al., 1991), and to inventory landslides using SPOT satellite images (Cheng et al., 2004). Multi-temporal satellite images are increasingly used to monitor, classify and detect landslides (Hervas et al., 2003; Mantovani et al., 1996).

For landslide analyses, Landsat™ and Advanced Spaceborne Thermal Emission and Reflection Radiometer (ASTER) have been used to derive land cover in regions including the Himalayas range (Saha et al., 2002; Sarkar & Kanungo, 2004; Zomer et al., 2002). InSAR has been used to locate and characterize landslides (e.g., Canuti et al., 2004; Singhroy & Molch, 2004). Kaab (2005) showed that recent Shuttle Radar Topography Mission (SRTM) results are promising for characterizing topography in regions having landslides. Pelletier et al. (1997) indicated that continuous remote-sensing of soil moisture coupled with a digital elevation model is a necessary component of a successful landslide hazard mitigation program. Their work recommended replacing soil moisture surrogates that have been used extensively in slope stability analyses and landslide observations. Typically, slope stability is analyzed using wetness indices to estimate soil wetness (Acharya et al., 2006; de Vleeschauwer & De Smedt, 2002; Montgomery & Dietrich, 1994; van Westen & Trelirn, 1996). As

* Corresponding author. 5500 Campanile Dr. San Diego, CA 92182, USA. Tel.: +1 619 594 0929; fax: +1 619 594 8078.
E-mail address: ramlakhan37@gmail.com (R.L. Ray).

0034-4257/$ – see front matter © 2010 Elsevier Inc. All rights reserved.
doi:10.1016/j.rse.2010.05.033

pointed out by Rosso et al. (2006), these approaches neglect the presence of soil moisture in the upper soil layer above the groundwater table (unsaturated soil layer or surface soil layer) or indirectly estimate the soil moisture. Existing studies do not directly account for the temporal evolution of soil moisture prior to and during the rainfall events. Nevertheless, it is necessary to link the surface soil moisture to the subsurface layer (saturated soil layer) because landslides are not triggered only by surface layer saturation; rather, it is the combined effect of surface and subsurface saturation that is critical (Ray & Jacobs, 2007). Ray et al.'s (2010) enhanced wetness index model provides a means to apply vadose zone soil moisture. While they used modeled soil moisture, many regions lack the required datasets for steep terrains that are needed to appropriately parameterize models. Remotely sensed soil moisture data are a potentially viable alternative to modeled data because they are available globally with frequent overpasses.

Satellite remote sensing can provide spatially integrated information on soil moisture at regional and global scales (Gruhier et al., 2010). There are various active microwave sensors such as Meteorological Operational Satellite Program (METOP)-Advanced Scatterometer (ASCAT), RADARSAT 1, 2-Synthetic Aperture Radars (SAR), Environmental Satellite (ENVISAT)-Advanced SAR (ASAR) and passive microwave sensors such as Advanced Microwave Scanning Radiometer (AMSR-E), Tropical Rainfall Measuring Mission (TRMM)-TRMM Microwave Imager (TMI), Soil Moisture and Ocean Salinity (SMOS, from Nov-2009) that are in operation to measure soil moisture at various spatial and temporal resolutions (Lakhankar et al., 2009). Until now, most of the satellites are producing soil moisture data at a course resolution. However, the proposed Soil Moisture Active and Passive (SMAP) that is scheduled to launch in 2014, will provide higher resolution soil moisture products (Gruhier et al., 2010).

While no landslide studies thus far have used remotely sensed soil moisture data, the AMSR-E soil moisture product has the potential to characterize soil moisture profiles in landslide prone regions (Ray & Jacobs, 2007). Numerous studies (e.g., Gao et al., 2006; Lacava et al., 2005; Njoku & Chan, 2006; Njoku et al., 2003; Walker et al., 2004) have shown that microwave remote-sensing measurements including AMSR-E are affected by surface roughness, topographic features, dense vegetation and soil texture. This indicates that soil moisture data may have limited value on steep topography (Njoku et al., 2000). The few validation experiments, such as Soil Moisture Experiments 2004 (SMEX04) in northern Sonora, Mexico (Jackson et al., 2008; Vivoni et al., 2008), that have been conducted on such terrain show that rocky slopes can mask the moisture signal.

There are two significant challenges to using AMSR-E data. The AMSR-E retrievals provide measured soil moisture for an upper thin surface (less than 5 cm) of the Earth (Jones et al., 2009; McCabe et al., 2005; Schmugge et al., 2002). This thin layer soil moisture information may not truly represent the entire soil moisture profile underneath thick soil layer (subsurface) above the bed rock. To obtain a soil moisture profile, it may be necessary to combine remotely sensed soil moisture with modeled soil moisture such as that from a soil vegetation atmosphere transfer (SVAT) model. Moran et al. (2004) demonstrated that SAR soil moisture with SVAT modeled soil moisture can accurately estimate the soil moisture profile. In addition, Drusch (2007) suggested that remotely sensed surface soil moisture is directly linked with model's surface soil moisture and can be combined to use in soil moisture analysis.

Another challenge is that AMSR-E processed data or EASE-gridded daily L3 soil moisture products have a 25 km spatial resolution (Gruhier et al., 2010). This is quite coarse for landslide studies even at regional and global scales. Therefore, it may be prudent to downscale the low resolution AMSR-E soil moisture to a finer scale. Wagner et al. (2008) developed a downscaling technique based on temporal stability of soil moisture. Doubkova et al. (2008) applied their technique to downscale European Remote Sensing (ERS) scatterometer soil moisture data from 50 to 1 km spatial resolution. Surface wetness index approaches based on land surface temperature (LST) and normalized vegetation index (NDVI) are appropriate means to downscale AMSR-E soil moisture from 25 to 1 km spatial resolution (Hemakumara et al., 2004; Hossain & Easson, 2008). Chauhan et al. (2003) included albedo in addition to NDVI and LST to downscale soil moisture. Their approach was enhanced by Yu et al. (2008) and found to provide a strong relationship between the downscaled and original AMSR-E soil moisture ($R^2 = 0.74$).

Here, we test the AMSR-E soil moisture product's ability to provide the vadose zone soil moisture estimates necessary to dynamically map landslide susceptibility. The study region, Cleveland Corral, California, US, is an active landslide area. The research objectives of this paper are (1) to compare AMSR-E and variable infiltration capacity (VIC-3L) surface soil moisture, and (2) to analyze the impacts in landslide susceptibility map using AMSR-E and VIC-3L surface soil moisture. Results consider AMSR-E 25 km pixels as well as downscaled 1 km pixels.

2. Theoretical approach

2.1. Slope stability model

This study uses the modified infinite slope stability model (Ray et al., 2010) to quantify landslide susceptibility including the vadose zone soil moisture and groundwater effects. The model assumes a pervious soil layer above an impervious soil layer or bed rock that has no vertical groundwater flow from the bottom of the soil layer. The infinite slope method (Skempton & DeLory, 1957), widely applicable for shallow slope stability analysis, calculates safety factors as the ratio of resisting forces to driving forces. The infinite slope stability model (Fig. 1) as adapted by the several researchers is

$$FS = \frac{C_s + C_r}{\gamma_e H \sin\theta} + \left(1 - m\frac{\gamma_w}{\gamma_e}\right)\frac{\tan\varphi}{\tan\theta} \quad (1)$$

where C_s and C_r are the effective soil and root cohesion [kN/m^2], γ_e is the effective unit soil weight [kN/m^3], H is the total depth of the soil above the failure plane [m], θ is the slope angle [°], m is the wetness index [adimensional], ϕ is the angle of internal friction of the soil [°], and γ_w is the unit weight of water [kN/m^3]. The effective unit soil weight is estimated as

$$\gamma_e = \frac{q\cos\theta}{H} + (1-m)\gamma_d + m\gamma_s \quad (2)$$

where q is any additional load on the soil surface [kN/m^2] and γ_d is dry unit soil weight [kN/m^2] for the unsaturated soil layer.

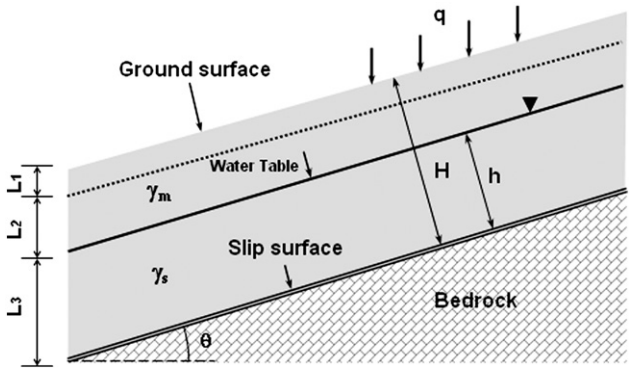

Fig. 1. Schematic diagram for the slope angle, saturated and total soil thickness, surcharge, saturated and moist unit soil weights (adapted and modified from Skempton & Delory, 1957). The three soil layers used in the VIC-3L model are the top soil layer, L1 = 0.05 m, the middle soil layer, L2 = 0.35 m and a variable depth lowest soil layer, L3 = 0.4 to 1 m. In the presented slope stability model, h and H are used for saturated and total soil depth, respectively.

The wetness index model following Ray et al. (2010) is given as

$$m = \frac{h + (H-h)^* \frac{\theta_s}{\eta}}{H} \quad (3)$$

where h is the saturated thickness of the soil above the failure plane [m], θ_s is the volumetric soil moisture [cm^3/cm^3] and η is the porosity [cm^3/cm^3].

The estimated factor of safety (FS) values were used to categorize slopes into stability classes using Pack et al. (1998) and Acharya et al.'s (2006) stability classification system. Our four susceptibility classes, used to develop landslide susceptibility map, are highly susceptible ($FS \leq 1$), moderately susceptible ($1 < FS < 1.25$), slightly susceptible ($1.25 < FS < 1.5$) and not susceptible (stable) ($FS \geq 1.5$).

2.2. Land surface model (VIC-3L)

This study used VIC-3L model results for the Cleveland Corral, California study region as an independent measure of the soil moisture profile. The VIC-3L model (Cherkauer & Lettenmaier, 1999; Liang et al., 1994, 1996, 1999) is a three-layer SVAT land surface scheme (Lohmann et al., 1998) that has been widely applied for surface runoff generation and soil moisture profile estimation (Dengzhong and Wanchang; Liang & Xie, 2003; Yuan et al., 2004). This macroscale land surface model simulates water and energy budgets and includes spatially variable soils, topography, precipitation, and vegetation. VIC-3L models water dynamics at scales ranging from a fraction of degree to several degrees or latitude and longitude (Maurer et al., 2002). The model can represent sub-grid variability in land surface vegetation classes, soil moisture storage capacity, topography as well as precipitation (Huang & Liang, 2006; Nijssen et al., 2001; Yuan et al., 2004; Zhou et al., 2004). Soil moisture storage, evapotranspiration, runoff and snow water equivalent are estimated at hourly to daily time-steps. VIC-3L uses the variable infiltration capacity approach (Nijssen et al., 1997) and varies runoff generation and evapotranspiration based on topography, soil and vegetation (Wood et al., 1992).

The VIC-3L soil column has three layers (Fig. 1) (Parada & Liang, 2004). The top, thin soil layer and the middle soil layer characterize the dynamic response of the soil to weather and rainfall events. The lowest layer captures the seasonal soil moisture behavior (Huang & Liang, 2006; Liang et al., 1996) and only responds to rainfall when the upper layer is wet. Precipitation infiltrates through the first soil layer to the second soil layer by gravity using the Brooks and Corey (1988) relationship (Lohmann et al., 1998). Base flow from the third soil layer contributes to runoff based on the ARNO model (Francini & Pacciani, 1991) with no downward groundwater flow from this layer.

The VIC-3L model characterizes $N + 1$ land cover types where N is the different land cover types and 1 represents bare soil. Each land cover type has a leaf area index (LAI), minimum stomatal resistance, roughness length, displacement length and relative fraction of root (Liang et al., 1994; Nijssen et al., 1997). This model uses the Penman–Monteith equation to calculate evapotranspiration at each grid cell (Nijssen et al., 1997).

The VIC-3L model can be operated in various simulation modes including an energy balance and water balance. The energy balance simulates the surface energy flux and solves the complete water balance. The water balance model, applied for this research, requires maximum and minimum temperatures, precipitation and wind speed data (Yulin et al., 2008; Zhou et al., 2004).

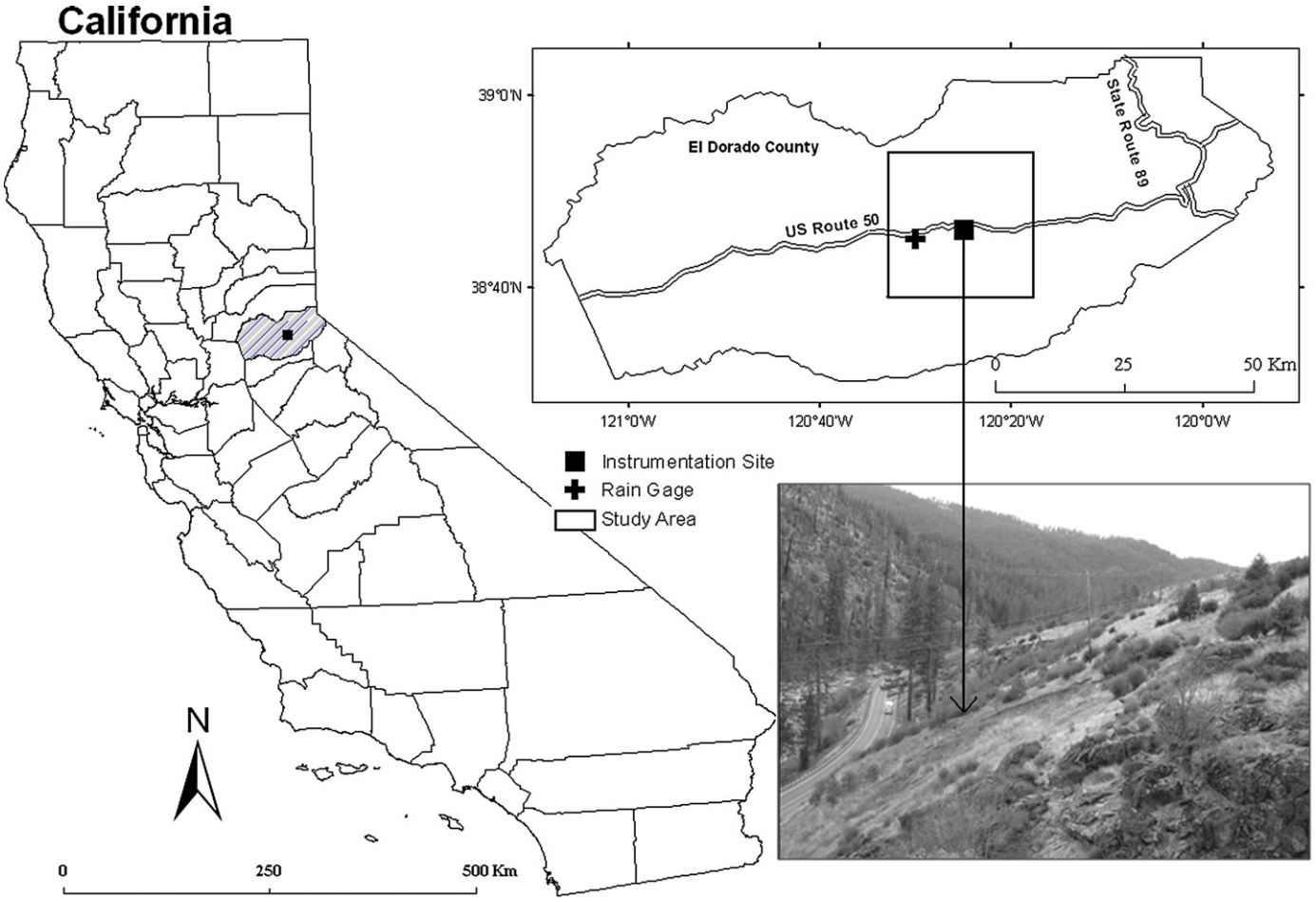

Fig. 2. The study region in El Dorado County in California with the mapped landslide.

3. Downscaling

For application to the infinite slope stability model, AMSR-E soil moisture can be used directly or downscaled. A linear or non-linear regression approach can be used to downscale the AMSR-E data from 25 to 1 km spatial resolution (Chauhan et al., 2003; Yu et al., 2008). Yu et al. (2008) found that it is possible to downscale AMSR-E soil moisture from 25 to 1 or 5 km spatial resolution using NDVI, albedo and LST. This paper uses Chauhan et al.'s (2003) approach to downscale the AMSR-E soil moisture from 25 to 1 km spatial resolution. The general downscaling approach proposed by Chauhan et al. (2003) and applied by Yu et al. (2008) is

$$\theta_s = \sum_{i=0}^{i=n}\sum_{j=0}^{j=n}\sum_{k=0}^{k=n} a_{ijk} V^i T^j A^k \quad (4)$$

where V is the NDVI, T is the LST and A is the albedo (1 km). The equation is applied with n = 1, yielding a simple linear equation with interaction terms

$$\theta_s = a_{000} + a_{001}A + a_{010}T + a_{100}V + a_{011}TA + a_{101}VA + a_{110}VT. \quad (5)$$

The AMSR-E (25 km) values and the NDVI, LST and albedo values, aggregated to a 25 km resolution, are used to determine the regression coefficients for the linear regression model. Following Yu et al. (2008), the 1 km NDVI, LST and albedo products are aggregated to 25 km spatial resolution by

$$V_{25} = \frac{\sum_{i=1}^{n}\sum_{j=1}^{m} V_{ij}}{mn}, \quad T_{25} = \frac{\sum_{i=1}^{n}\sum_{j=1}^{m} T_{ij}}{mn}, \quad A_{25} = \frac{\sum_{i=1}^{n}\sum_{j=1}^{m} A_{ij}}{mn} \quad (6)$$

where V_{25} is the 25 km average NDVI, T_{25} is the 25 km average LST, A_{25} is the 25 km average albedo and m and n are, respectively, the number of 1 km pixels in *i*th rows and *j*th columns in the AMSR-E pixel.

Once a regression model is established, the model is applied to estimate the 1 km soil moisture from the 1 km NDVI, LST and albedo values. The downscaled AMSR-E (1 km) can be re-aggregated to a 25 km resolution and compared with observed AMSR-E (25 km) to quantify the model error.

4. Methods and data

4.1. Study region

The Cleveland Corral study region in Highway 50 corridor is located in the Sierra Nevada Mountains, California, USA (Reid et al., 2003). Highway 50 is a major road located between Sacramento and South Lake Tahoe in California (Spittler & Wagner, 1998). Fig. 2 shows observed recent landslide and location of study domain in California. The investigated area is about 28 by 22 km (616 km^2) with elevations that range from about 902 to 2379 m. Since 1996, slope movement and landslides occur infrequently during winter season. Additionally, one major catastrophic landslide occurred in 1983 (Spittler & Wagner, 1998). Since 1997, the United State Geological Survey (USGS) has monitored this region using real time data acquisition systems (Reid et al., 2003). They found elevated pore-water pressures and wet soils cause slope movement and landslides during the winter (rainy) season.

Table 1 summarizes the study region's soils, land cover and climate. The predominant soil is sandy loam (72%). The total soil depth ranges from 0.6 to 1.4 m. Underneath the soil layer, the potential failure plane is bedrock. Conifer and wooded grassland are the dominant land covers, 80% and 14% of the study region, respectively. Some rock outcrops were also observed along the Highway 50 corridor. The north-east part of the study area has limited data because of water bodies and rock outcrops. This region has an average annual rainfall of 1101 mm, with 725 mm occurring during the winter.

Table 1
Soil, vegetation, slope and climate characteristics for the Cleveland Corral, California, US study area.

California	
Land cover	Area (%)
Evergreen forest	3.3
Conifer	79.9
Deciduous forest	2.7
Wooded grassland	14.1
Soil texture	
Sandy loam	72.0
Loam	16.0
Sandy clay	3.0
Clay loam	9.0
Slope (°)	
0–15	71.2
15–30	27.5
30–45	1.2
45–60	0.0
Climate	
Average annual rainfall (mm)	1101.0
Average rainfall wet season (mm, Jan–May)	725.0
Average maximum temperature (°C)	19.6
Average maximum temperature (°C)	5.5

4.2. Remotely sensed data

4.2.1. AMSR-E soil moisture

The AMSR-E instrument was developed by the National Space Development Agency of Japan (NASDA) and launched on the Aqua satellite by the National Aeronautics and Space Administration (NASA) on May 4, 2002 (Li et al., 2004). It measures radiation at six frequencies in the range 6.9–89 GHz (Njoku et al., 2003). Lower frequencies, L band (1–2 GHz), are more sensitive to soil moisture, but they are more susceptible to dense vegetation and radio frequency interference (RFI). The higher frequency C (6.9 GHz) and X (10.65 GHz) bands can be used to retrieve soil moisture (Jackson et al., 2005) because these higher frequency bands are comparatively less susceptible to RFI. The AMSR-E directly measures brightness temperature. Soil moisture retrievals use a radiative transfer (RT) model that links surface geophysical variables to the observed brightness temperature (Njoku et al., 2003). An RT model initially assumes a soil moisture value and predicts the brightness temperature based on surface parameters, vegetation parameters, and sensor parameters. If the difference between the predicted brightness temperature and the observed temperature is less than acceptable limit, then the final soil moisture value is derived. Otherwise the iteration continues with a modified initial soil moisture value. A detailed description of the retrieval algorithm appears in Njoku et al. (2003).

AMSR-E level 3 products (e.g., surface soil moisture, vegetation water contents, etc.) are developed from the level 2B product's brightness temperature at a 25 km Earth grid scale both for ascending and descending passes.

(http://www.ghcc.msfc.nasa.gov/AMSR/data_products.html). This study used the ascending pass AMSR-E soil moisture level 3 products from Jan 1, 2003 to Dec 31, 2006 on a daily basis. AMSR-E level 3 products were obtained from NASA Earth Observing System Data Gateway through the National Snow and Ice Data Center (NSIDC).

4.2.2. MODIS data

The Moderate Resolution Imaging Spectroradiometer (MODIS) instrument developed by NASA was launched on the Terra satellite in

December 1999 and on the Aqua satellite in May 2002 (Wang et al., 2009). MODIS can collect information both in the morning and in the afternoon as Terra is scheduled to pass from north to south across the equator in the morning and Aqua is scheduled to pass from south to north in the afternoon. Even though Terra and Aqua satellites pass in the morning and in the afternoon, respectively, the temporal resolution of MODIS products is only every 1 to 2 days (Luo et al., 2008). MODIS data are available at spatial resolutions of 0.25, 0.50, and 1.0 km as well as coarser resolutions (Luo et al., 2008).

This study required NDVI, albedo and LST at a 1 km spatial resolution. The 1 km MODIS TERRA albedo (MCD43B3), NDVI (MYD13A2) and LST (MYD11A1) products were used to downscale the AMSR-E surface soil moisture for 2005. Monthly LAI values, used in VIC-3L model, were obtained from the MODIS. The MOD15A2, 8-day composite LAI values were averaged to monthly values. These data are available as tiles in the Sinusoidal (SIN) projection. All these data were re-projected into a geographical projection.

4.3. Model data

The soil and vegetation parameter required for the slope stability model were obtained from the States Soil Geographic (STATSGO) (Soil Survey Staff, 2008), Land Data Assimilation System (LDAS; Mitchell et al., 2004) as well as from the literature (Table 2). Root cohesion enhances the shear strength of soil and acts as a resisting force against sliding. Root cohesion values for each vegetation class were adapted from Sidle and Ochiai (2006). The unit soil weight (saturated and dry) was calculated based on the soil moisture, soil porosity, and specific gravity of the soil samples using methods adapted by Ray et al. (2010). Each soil type was assigned soil cohesion and friction angle values based on Deoja et al. (1991) and the slope of the retention curve from Clapp and Hornberger (1978). Similarly, soil bulk density, field capacity, wilting point and saturated hydraulic conductivity values were from Miller and White (1998) and Dingman (2002). A 90 m SRTM digital elevation model (DEM) was used to calculate slope angle.

For this region, validation data for landslide studies are difficult to obtain. Daily groundwater measurements were obtained from the USGS which uses piezometers to measure the hydraulic head at one of the active landslides in the region. (Mark Reid, USGS, personal communication, April 23, 2007). Previous research indicates that over 600 small to large landslides have occurred in this study region (Reid et al., 2003; Spittler & Wagner, 1998). In addition, field observations identified 10 locations where failures had occurred prior to December 2007. Table 4 lists slide locations and their physical characteristics. Observations show that most of the mapped landslides were located in woodland regions with sandy loam soil texture. The slopes of the mapped landslides range from 24° to 37°.

Table 2
List of model parameters and sources by model.

Parameters	Sources	Model
Soil cohesion	Deoja et al. (1991)	Slope stability
Soil porosity	Dingman (2002)	Slope stability and VIC-3L
Soil texture	STATSGO	Slope stability and VIC-3L
Soil depth	STATSGO	Slope stability and VIC-3L
Hydraulic conductivity	STATSGO	VIC-3L
Soil bulk density	Dingman (2002)	Slope stability and VIC-3L
Angle of internal friction	Deoja et al. (1991)	Slope stability
Additional load (surcharge)	Ray (2004)	Slope stability
Land cover	University of Maryland	Slope stability and VIC-3L
Root cohesion	Sidle and Ochiai (2006)	Slope stability
Root depth	LDAS	VIC-3L
Root fraction	LDAS	VIC-3L
Vegetation roughness	LDAS	VIC-3L
Vegetation height	LDAS	VIC-3L
Leaf area index (LAI)	MODIS	VIC-3L
Rainfall	NCDC	VIC-3L
Groundwater	USGS	Slope stability
Temperature	NCDC	VIC-3L
Wind speed	NCDC	VIC-3L

STATSGO = States Soil Geographic, LDAS = Land Data Assimilation System, USGS = United States Geological Survey, VIC-3L = Variable Infiltration Capacity-3 Layers. NCDC = National Climatic Data Center.

4.4. Analysis methods

A course resolution AMSR-E (25 km) was downscaled to fine (1 km) resolution using MODIS LAI, albedo, and NDVI at 1 km spatial resolution. Using time series analysis, AMSR-E soil moisture at 25 km resolution was compared with VIC-3l model surface soil moisture (layers 1 and 2) at 1 km spatial resolution to study the soil moisture variability in study area. Because no in-situ soil moisture measurements were available, daily groundwater measurements were also compared with AMSR-E and VIC-3l model soil moisture. The maximum model saturation day, 8 May, 2005, was identified to develop landslide susceptibility map. To address the low variability of AMSR-E soil moisture, downscaled AMSR-E soil moisture was scaled from residual soil moisture (minimum) to soil porosity (maximum).

This study uses a 90 m spatial resolution to calculate wetness index, dry unit soil weight, effective unit soil weight and factor of safety. The effective unit weight of soil was calculated using dry unit weight, wetness index, depth of soil, surcharge and slope angle (Eq. (2)). Wetness indices were calculated using Eq. (3) for modeled groundwater depth on May 8, 2005 (maximum saturation) and the groundwater table located at midpoint of the soil layer (half saturation) with the 1 km VIC-3L model vadose zone soil moisture values as well as the 1 and 25 km resolution AMSR-E soil moisture values.

Finally, safety factors were calculated for these two groundwater positions using VIC-3L model soil moisture and AMSR-E soil moisture. Theoretically, landslides occur when the safety factor is less than one. The estimated FS values were used to categorize slopes into the four landslide susceptibility classes; highly susceptible, moderately susceptible, slightly susceptible and stable.

5. Results and discussion

5.1. Downscaling AMSR-E soil moisture

AMSR-E soil moisture at Cleveland Coral, California was downscaled from 25 to 1 km using daily data from January 1 to December 31, 2005. The 1 km NDVI, LST, and albedo were aggregated to 25 km resolution using Eq. (6). The observed maximum LST, albedo and NDVI are, respectively, 51 °C, 0.94 and 0.93. The minimum are, respectively, −20 °C, 0.01 and −0.14. The AMSR-E (25 km) was regressed with aggregated NDVI, LST and albedo values (Eq. (5)). The estimated regression coefficients for each individual parameter and interaction term were used to develop Eq. (7). The regression model which best fits the soil moisture observation is

$$\theta_s = -1.426 + 4.169\ A + 0.006\ T + 2.254\ V - 0.017\ TA + 0.781\ VA - 0.009\ VT \quad (7)$$

This regression model provided a good fit with an R^2 of 0.73, a root mean square error (RMSE) of 0.009 cm^3/cm^3 and p-values less than 0.0001 for all independent variables. As anticipated, soil moisture increases with increasing vegetation index. However, the model associates wetter soils with higher albedo values and higher temperatures in contrast to typically observed physical relationships. Because this equation describes the annual cycle of surface and moisture conditions, the model interaction terms are very important. The soil moisture variability is described primarily by the vegetation index changes and the interactions between vegetation and albedo. The

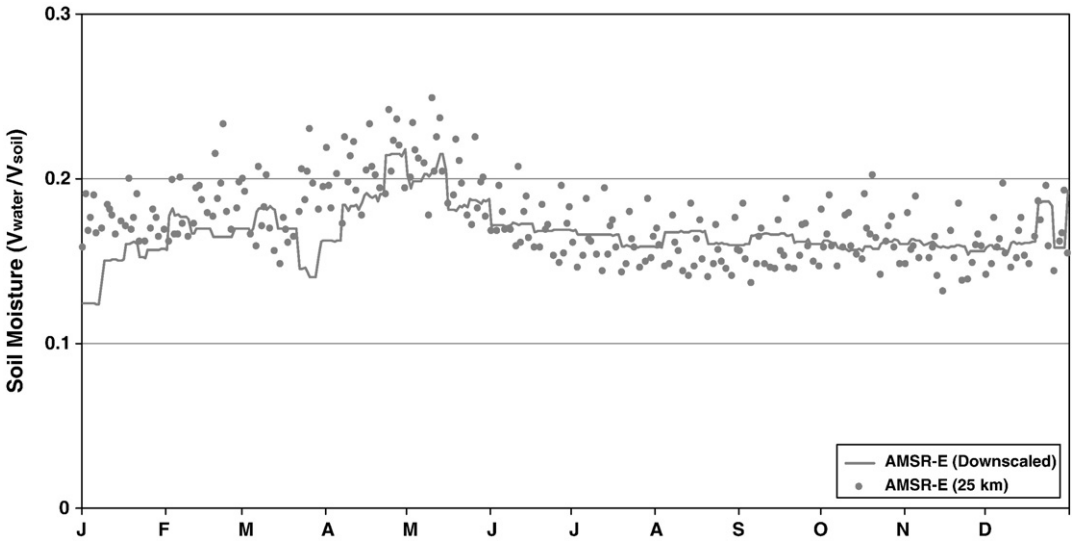

Fig. 3. Daily observed AMSR-E (25 km spatial resolution) and downscaled AMSR-E (1 km spatial resolution) aggregated to 25 km spatial resolution in 2005 at Cleveland Corral, California, US. $R^2 = 0.58$, RMSE = 0.017 cm^3/cm^3.

interaction terms between temperature and albedo, as well as vegetation and temperature are critical to understanding the role of albedo and surface temperature.

The resulting model was used to estimate the 1 km soil moisture values. These values were aggregated to 25 km and compared to the AMSR-E observed soil moisture values (Fig. 3). The results show very good agreement between the observed and the downscaled AMSR-E soil moisture. A moderate correlation was observed with an R^2 of 0.58 and a small RMSE of 0.017 cm^3/cm^3. The results are comparable to Yu et al.'s (2008) R^2 values that ranged from 0.19 to 0.74 with 6 different regression techniques and Chauhan et al.'s (2003) RMSE of 0.016 cm^3/cm^3.

Both the downscaled (1 km) and the observed AMSR-E soil moistures (25 km) capture the seasonal variations of moisture. The observed and downscaled soil moisture values are high during the winter wet season. However, a small time lag between the 25 km AMSR-E values and the downscaled soil moisture is evident during the wet season. The time lag is about a week. This time lag may be due to two types of errors (Chauhan et al., 2003). The first error is due to regression analysis and the second error is associated with input data. They found a regression error in analysis and precision error in NDVI, albedo and LST. Overall, the results suggest that reasonable downscaled AMSR-E soil moisture can be produced using 1 km MODIS LST, albedo and NDVI values. In the future, it is recommended that independent validations be performed using in-situ soil moisture measurements for the 1 km spatial scale.

5.2. Comparison between observed AMSR-E and VIC-3L soil moisture

Fig. 4 shows the observed AMSR-E soil moisture, the VIC-3L model's 1st and 2nd layers soil moisture, in-situ groundwater measurements and snow accumulation at an active landslide pixel. The VIC-3L's first and second soil layer thicknesses were 0.05 and 0.35 m, respectively. Both VIC-3L and AMSR-E estimate higher surface soil moisture during the rainy season and lower soil moisture values during the dry season. The results show minimal differences between the first and second layers' soil moistures estimated by the VIC-3L model. This suggests that the surface moisture is an indicator of the vadose zone soil moisture profile for this region. For a shallow slope stability analysis, the unsaturated soil layer is often a comparatively thin layer.

As shown in Fig. 4, snow occurs regularly from December to March. AMSR-E does not completely capture the soil moisture variability when there is snow. When snow is present on the ground, the surface temperature is often below 0 °C. At this freezing temperature, the dielectric constant is very small and AMSR-E soil moisture retrievals are not possible (Hallikainen et al., 1985; Wang et al., 2009). For this region, lower or no soil moisture is indicated by AMSR-E every year in early winter. Thus, it is recommended that operational in-situ or remotely sensed snow monitoring be used in combination with AMSR-E soil moisture for landslide studies in snowy regions.

Because no in-situ soil moisture measurements were available, modeled and AMSR-E soil moisture values were compared to groundwater measurements. Although groundwater, AMSR-E and modeled soil moisture values are different measures, their temporal evolution is similar during the wet season. If the snow period is not taken into account, both AMSR-E and VIC-3L model predicted that mid April to mid May is consistently very wet. For example, the maximum soil moisture predicted by AMSR-E and VIC-3L model were 0.25 (cm^3/cm^3) and 0.37 (cm^3/cm^3) on May 10 and 8 in 2005, respectively.

Another challenge is that the AMSR-E soil moisture measurements are lower during the wet season as compared to the VIC-3L measurements and have much lower variability overall. For example, between the dry and wet periods, the soil moisture increase observed by AMSR-E was about 50% whereas VIC-3L model estimated a 75% increase. Some of this difference may be caused by the layer thicknesses. AMSR-E's 0–2 cm thin soil layer may dry faster than the VIC-3L's 5 cm soil layer. Previous research shows that the AMSR-E soil moisture estimates are lower than land surface models and measured values (Choi et al., 2008; Gruhier et al., 2008; Sahoo et al., 2008). These limitations are particularly apparent for dense vegetation, steep terrain and due to the course resolution of AMSR-E products.

Overall, the AMSR-E soil moisture measurements can capture the timing of the modeled soil moisture wetting. However, the degree of wetness is considerably different and further complicated by snow.

5.3. Scaling (AMSR-E)

Reichle et al. (2004) suggest that the satellite soil moisture values be scaled using modeled data. Choi and Jacobs (2008) found that the AMSR-E soil moisture can be scaled to match in-situ as well as modeled land surface wetness. To address the low variability of the AMSR-E surface soil moisture, the observed AMSR-E values were scaled, then compared to the VIC-3L surface soil moisture.

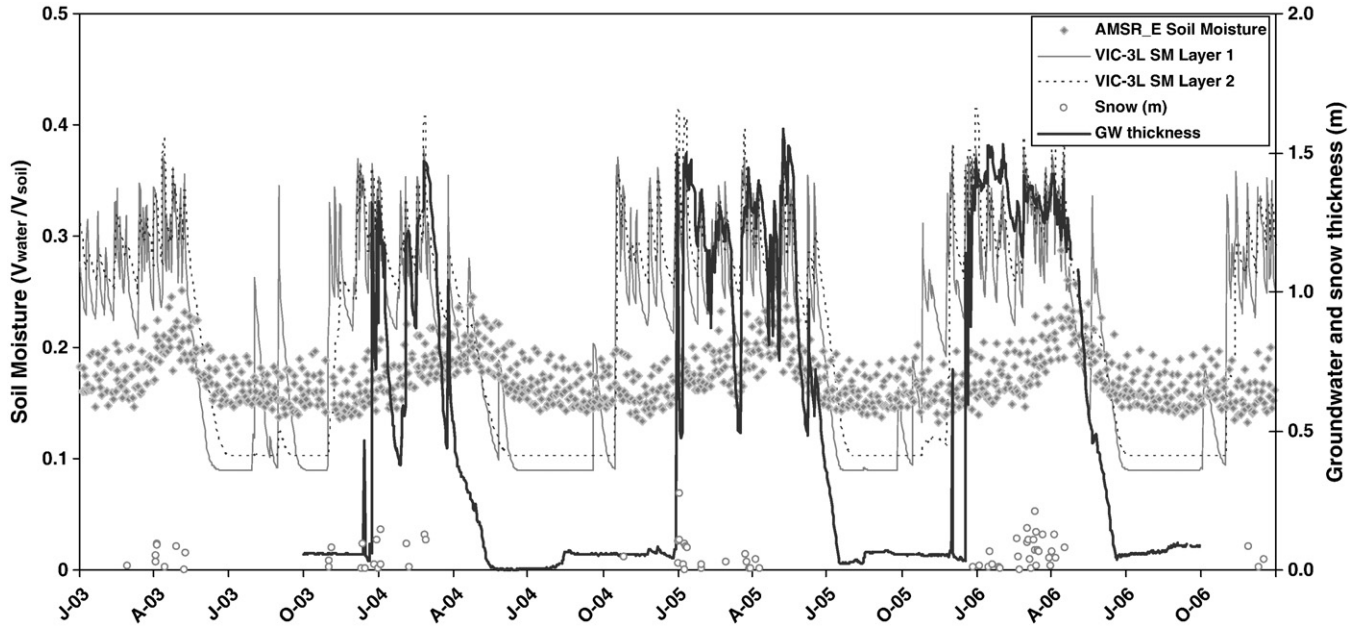

Fig. 4. Observed AMSR-E soil moisture, VIC-3L soil moisture layer (1 and 2), snow and groundwater measurements at Cleveland Corral, California, US. Groundwater thickness is measured from the bottom of piezometer installed at 1.82 m below the surface.

AMSR-E soil moisture was scaled to minimum and maximum values using a simple interpolation approach. The minimum and maximum observed AMSR-E soil moisture values were 0.09 and 0.33 cm^3/cm^3 in 2005, respectively. For the sandy loam soils in Cleveland Corral, California, a residual saturation of 0.05 suggested by Rawls et al. (1982) and an upper bound equal to the 0.48 soil porosity were used. AMSR-E soil moisture values were scaled from 0.05 to 0.48 cm^3/cm^3. Based on these two end values, a linear relationship was established between the observed AMSR-E values and the scaled values. This linear relationship was applied to each raw AMSR-E soil moisture value to obtain a scaled AMSR-E soil moisture value.

Fig. 5 shows promising agreement between the VIC-3L soil moisture and the scaled AMSR-E soil moisture. With the scaling, AMSR-E has a soil wetness similar to that estimated by the VIC-3L model during the dry and wet seasons with overall improved variability. Using Eq. (3), the scaled AMSR-E provides higher wetness index estimates than from the un-scaled AMSR-E soil moisture. Without scaling, it may not be possible to capture actual wetness of soil layer by AMSR-E in this study region. However, this may not be true in other locations and the approach to scaling remains an open question. While the snow challenges are still evident, soil moisture values are still consistent during the critical failure period, late spring.

5.4. Soil moisture variability

Soil wetness defined by groundwater and vadose zone soil moisture plays a critical role in slope instability. During the rainy season, rainfall increases soil moisture and groundwater table. With the constant slope and geotechnical parameters, soil saturation is the dynamic factor that causes slopes to become unstable because instability increases with increasing soil saturation. A slope becomes unstable when its soil saturation results in its safety factor falling below 1.

For the 3-year study period, the maximum saturation occurred on May 8, 2005. The maximum modeled saturation is the wettest day and had a groundwater table close to the surface and high vadose zone soil moisture. Fig. 6 shows AMSR-E (1 km) and VIC-3L (1 km) soil moisture distributions on May 8, 2005. The VIC-3L soil moisture values are somewhat higher than the AMSR-E values. The VIC-3L soil moisture values range from 0.25 to 0.52 whereas the AMSR-E downscaled, but un-scaled soil moisture values range from 0.09 to 0.33 (cm^3/cm^3). The scaled AMSR-E soil moisture ranges from 0.05 to 0.48 cm^3/cm^3 which is an increase of 0.15 cm^3/cm^3 at upper bound and very close to the VIC-3L upper bound soil moisture value.

Both AMSR-E and the VIC-3L model reveal similar soil moisture distribution patterns in the north-west and south-east corners as well as along Highway 50. The VIC-3L and AMSR-E show a low soil moisture values along the highway because the physical characteristics of the ground such as paved highway, numerous retaining and revetment walls, built up area and stream affects the quality of AMSR-E and VIC-3L modeled soil moisture estimates.

Differences in the soil moisture distribution were observed at the north-east and south-west corners of the study region. The north-east region has a number of physical features that appear to challenge the satellite soil moisture retrieval and the disaggregation approach. The observed brightness temperature is used to retrieve AMSR-E soil moisture. High albedo values were found in the north-east region (Fig. 7a). Thus, a lower brightness temperature and higher albedo caused by snow or bright exposed surface such as sand or bare rock may influence disaggregation. AMSR-E measurements are comparatively low in the south western corner of the study region. This area has the densest vegetation cover as evidenced by the high NDVI values (Fig. 7b). AMSR-E cannot provide reasonable measurements with dense vegetation (McCabe et al., 2005; Njoku & Chan, 2006) because of the sensitivity of the C- and X-bands to dense vegetation.

On May 8, 2005, the observed AMSR-E soil moisture value was 0.17 cm^3/cm^3 at the native 25 km scale. This 0.17 cm^3/cm^3 soil moisture value matches the average of the 1 km pixels in the study region. The simple downscaling model is promising. It captures much of the soil moisture variability in the study region with values ranging from 0.09 to 0.33 cm^3/cm^3 instead of the single 0.17 cm^3/cm^3 soil moisture value for the entire study region. In the future, higher resolution sensors and better downscaling approaches that can produce soil moisture at finer than 1 km may improve soil moisture estimation for landslide prone regions.

5.5. Susceptibility analysis

AMSR-E soil moisture values at the 25 and 1 km scale were used to calculate safety factors. These results were compared to safety factors

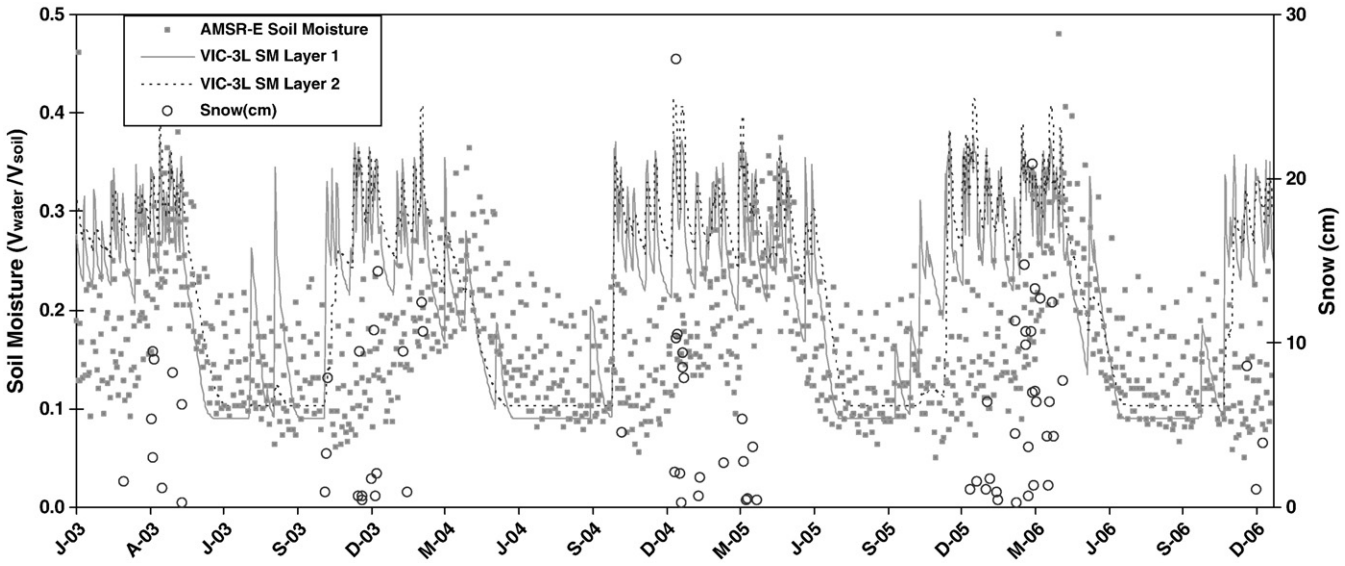

Fig. 5. Observed scaled (0.05–0.48 cm^3/cm^3) AMSR-E soil moisture, VIC-3L soil moisture layers (1 and 2) and snow values at Cleveland Corral, California, US.

estimated using VIC-3L soil moisture. This section presents regional landslide susceptibility results using AMSR-E and VIC-3L soil moistures. Three wetness scenarios were considered. The half saturation condition occurred on May 23, 2005. On this date, the vadose zone soil moisture varies spatially and the groundwater table was located at the middle of the soil. The maximum saturation, May 8, 2005, was discussed in the previous section. The full saturation scenario was not observed, but is presented to provide an upper bound to landslide susceptibility based on an assumed completely saturated profile.

Table 3 presents the predicted susceptible and stable areas using the AMSR-E soil moisture (25 and 1 km) and the VIC-3L soil moisture (1 km) for the three scenarios. As expected, the predicted susceptible areas for all saturation scenarios were below the fully saturated condition for both AMSR-E and VIC-3L soil moistures. Under the half and maximum modeled saturation scenarios, the predicted susceptible area with the VIC-3L soil moisture was slightly higher than that using AMSR-E soil moisture. This reflects the wetter VIC-3L vadose zone compared to the AMSR-E surface soil moisture under maximum saturation scenario. The results show that 0.41% and 0.49% of the area are highly susceptible using AMSR-E (25 km) and VIC-3L model (1 km) soil moisture, respectively.

A small prediction difference was observed with AMSR-E (25 km) and downscaled (1 km) soil moisture under half and maximum modeled saturation scenarios. This shows that it can also be appropriate to use AMSR-E observed soil moisture in slope stability analysis if downscaling is not possible or desirable. However, in comparison to the observed AMSR-E (25 km), the downscaled AMSR-

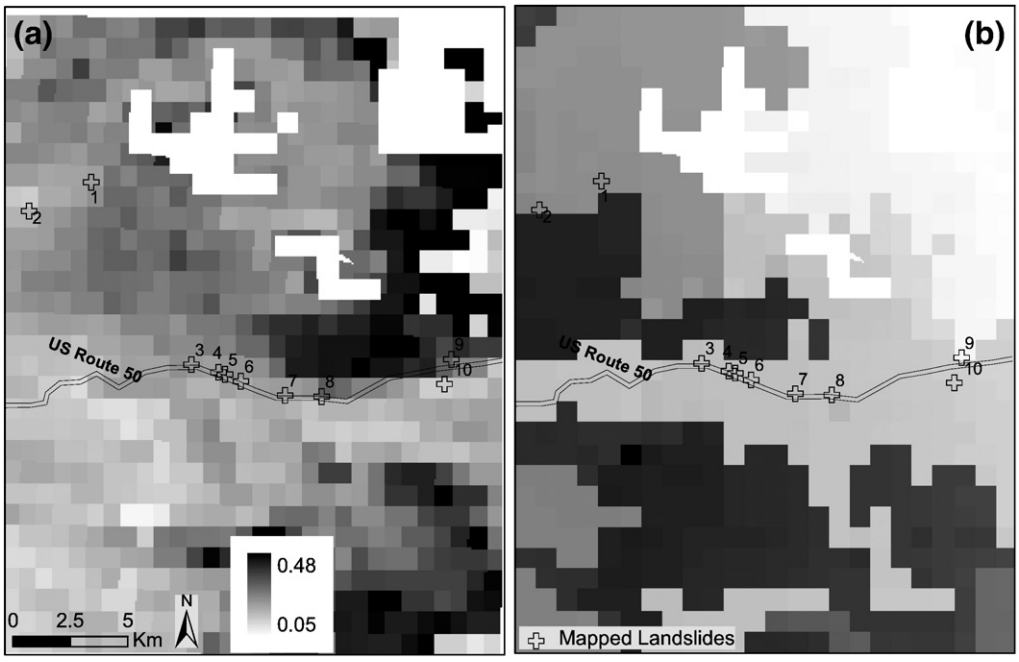

Fig. 6. Maximum modeled soil moisture day on May 8, 2005, (a) AMSR-E (b) VIC-3L.

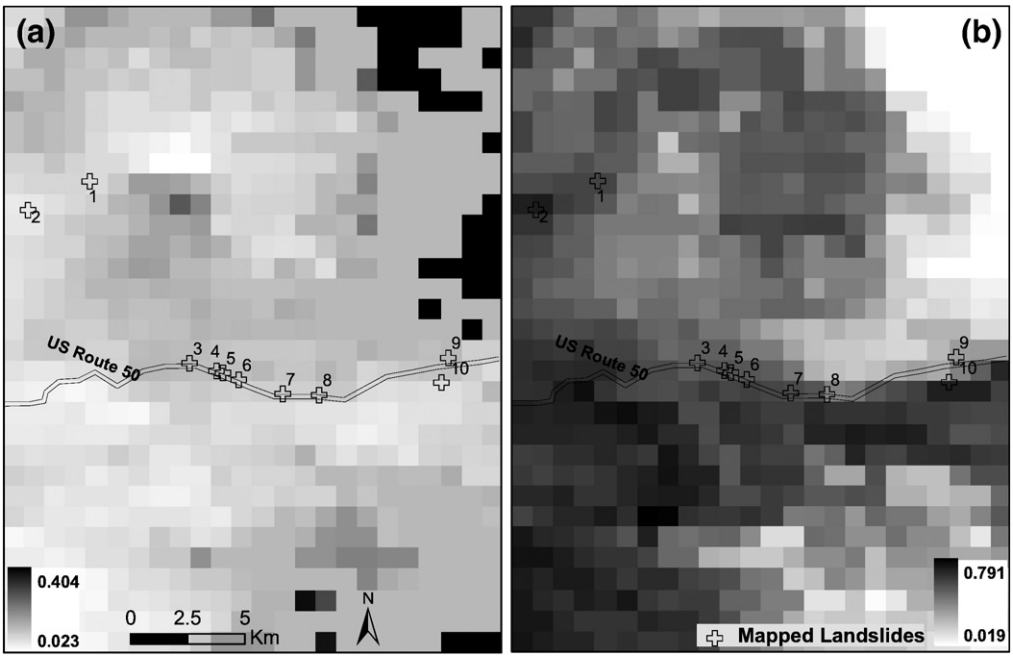

Fig. 7. On maximum modeled soil moisture day (May 8, 2005), (a) observed albedo at 1 km, (b) observed NDVI at 1 km.

E (1 km) may be more appropriate to use in slope stability analysis because higher resolution datasets are consistently recommended for landslide mapping.

Fig. 8 shows the susceptibility distributions by class for AMSR-E and VIC-3L soil moistures under the maximum modeled saturation scenario. Qualitatively, both VIC-3L and AMSR-E vadose zone soil moistures identified the same hazard zones as highly, moderately and slightly susceptible. However, small differences occur in the predicted susceptible areas (Fig. 9). 83.2% of highly susceptible locations predicted using VIC-3L vadose zone soil moisture were also identified as highly susceptible by AMSR-E. Most of those locations not successfully identified were adjacent to areas correctly predicted.

Because no methods exist to map an entire susceptible area for validation, this study compares observed historical and present landslides to the model results. The study area was surveyed to identify a series of landslide locations for validation (Table 4). Due to the study extent and terrain, the survey was not comprehensive or exhaustive. Ten landslide sites (nine historical and one active) were observed in this study area. At active landslide site, slope movements and landslides occurred in May 2005 and earlier.

Susceptibility maps were compared with the landslide inventory data. For the May 8, 2005 saturation conditions, six of the mapped landslide locations would have been considered highly unstable. On May 8, 2005, four of the mapped landslides were identified as moderately susceptible. Since, the exact dates of mapped landslides are unknown; it is possible that some of the landslides occurred when soil moisture was higher than maximum modeled soil moisture on May 8, 2005. Moreover, moderately susceptible areas are not stable zones. External forces such as of vibrations caused by an Earthquake, large tree shaking (due to wind) and heavy highway traffic can trigger a slope to fail in a moderately susceptible area. Interestingly, the four mapped landslides are located along the Highway 50 and any external forces that are not included in slope stability model can cause slope failure in moderately susceptible area.

In addition, soil cohesion, root cohesion and angle of internal friction that support stability are highly variable in space and time. This study adapted those parameters from the literature. A small variation in adapted value can change the susceptible area. For example, a 1% increase in soil cohesion, root cohesion and angle of internal friction reduced highly susceptible areas by 0.69%, 0.35% and 1.8%, respectively using the 1 km downscaled AMSR-E soil moisture on May 8, 2005 (Fig. 10). Root cohesion has a relatively small on stability because it is directly linked with vegetation cover which is not uniformly distributed in the study area. The two soil strength

Table 3
The portion of the study area (%) for each landslide susceptibility classification using VIC-3L, AMSR-E 25 km and downscaled soil moisture at Cleveland Corral, California, US. Three wetness scenarios are presented.

Scenario	Highly susceptible	Moderately susceptible	Slightly susceptible	Stable
Full saturation	0.58	1.90	3.01	94.51
Half saturation[a]				
VIC-3L (1 km)	0.31	1.14	2.32	96.23
AMSR-E (25 km)	0.24	0.90	1.96	96.90
AMSR-E (1 km)	0.22	0.95	2.13	96.70
Maximum modeled saturation[b]				
VIC-3L (1 km)	0.49	1.69	2.89	94.93
AMSR-E (25 km)	0.41	1.41	2.59	95.59
AMSR-E (1 km)	0.42	1.47	2.67	95.44

[a] Half saturation — groundwater position table at half of the soil layer (May 23, 2005).
[b] Maximum modeled saturation — the day having the groundwater was closest to the surface and wettest vadose zone (May 8, 2005).

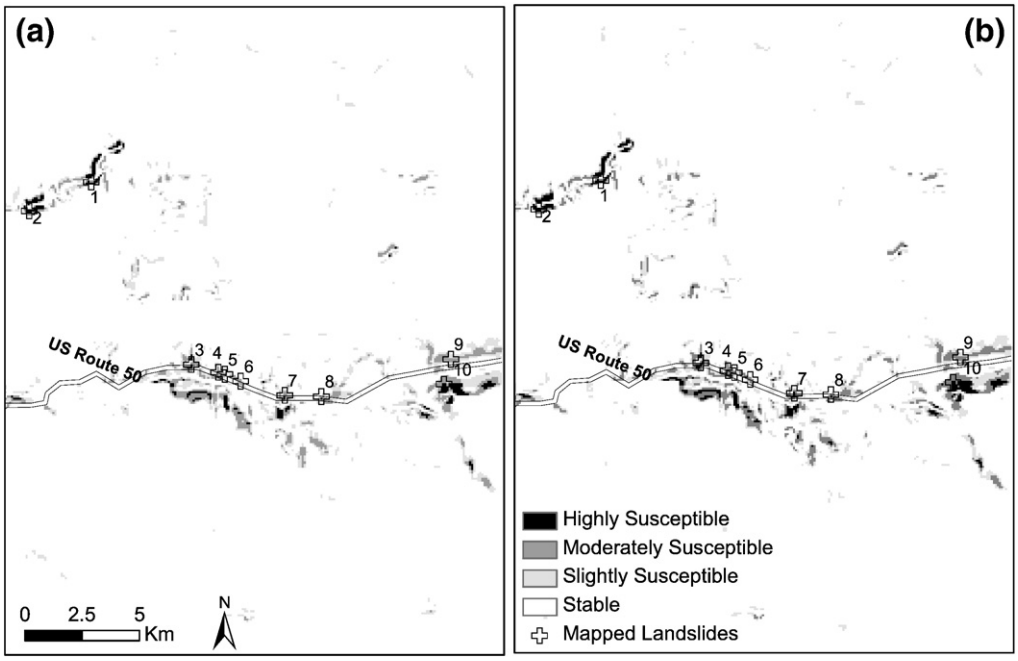

Fig. 8. Landslide susceptibility map for maximum modeled saturation day (May 8, 2005) using (a) AMSR-E soil moisture and (b) VIC-3L soil moisture.

parameters have greater impacts on slope stability. The soil cohesion only applies to cohesive soil whereas frictional angle applies both to cohesive and cohesionless soils. Because the study area has both cohesive and cohesionless soils, the impact of frictional angle on slope stability is greater than the soil cohesion. Moreover, the major part of the driving/destabilizing force caused by a slope angle is resisted by angle of internal friction. For example, the angle of internal friction in a cohesionless soil is equal to the angle of repose (angle at which the soil can settle naturally). Future landslide studies at large-scale remote-sensing studies will benefit from improved confidence in soil parameters.

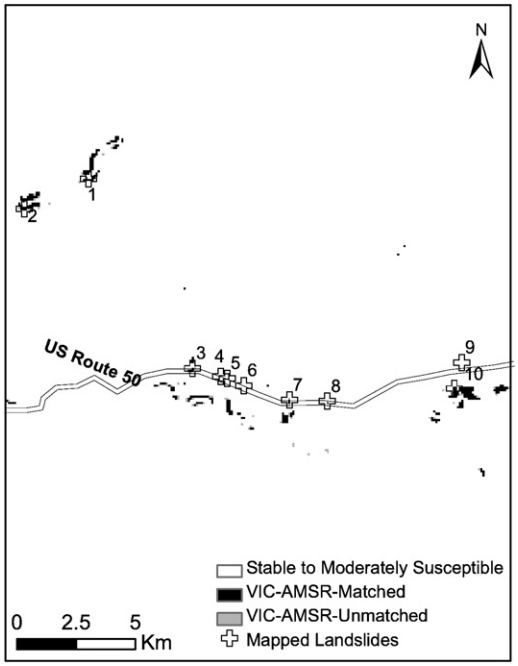

Fig. 9. Comparison of highly susceptible area predicted using VIC-3L and AMSR-E on maximum modeled soil moisture day (May 8, 2005). Black squares indicate identical predictions. Gray squares are location identified by VIC-3L highly susceptible, but not by AMSR-E.

6. Conclusion

This research used an infinite slope stability model with a pervious soil layer above the impervious soil layer or bed rock having no vertical groundwater flow from the bottom of the soil layer in combination with downscaled AMSR-E soil moisture measurements to map landslides. Through comparisons to VIC-3L model surface soil moisture and groundwater measurements, AMSR-E surface soil moisture was demonstrated to provide a quantitative estimate of vadose zone moisture for landslide susceptibility mapping at regional and global scales. Susceptibility maps for this study region were compared and validated with landslides inventory data and show promising agreement. The satellite-based products can provide an efficient means to develop landslide susceptibility maps based on antecedent soil moisture conditions.

While AMSR-E can provide surface soil moisture, there are challenges and significant research needs. Because AMSR-E had much lower soil moisture and less variability than would be expected, it was necessary to scale the AMSR-E soil moisture. In addition, the spatial scale of AMSR-E observations is much greater than the typical landslide scale. Downscaling provides some improvement, but better methods that can downscale AMSR-E soil moisture to finer than 1 km spatial resolution, are needed. Moreover, AMSR-E cannot produce reasonable soil moisture when there is snow on the surface. Finally, the lack of in-situ soil moisture on landslides prone slopes as well as observed slope failures coincident with soil moisture observations is a significant obstacle to validating results and enhancing hazard mitigation.

The ability to capture the evolution of soil moisture will allow us to anticipate critical hazard periods on an ongoing, real time basis. For developed nations, EOS measurements can complement existing physical databases by characterizing changing terrestrial systems and hydrologic stores. For less data rich regions, EOS measurements provide high resolution characterization of the Earth's surface. This approach is not recommended for local/hillslope scale slope stability analysis, but is very promising for regional and global scales.

Table 4
Physical characteristics and estimated safety factor (FS) of the mapped landslide's region. FS values were calculated under maximum modeled saturation conditions (May 8, 2005) and full saturation.

S.N.	Longitude	Latitude	Slope (°)	Land cover	Soil types	FS: Full saturation	FS: VIC-3L (1 km)	FS: AMSR-E (1 km)	FS: AMSR-E (25 km)
1	−120° 27′ 26″	38° 51′ 03″	27.4	Evergreen	Loam	0.753	0.770	0.797	0.799
2	−120° 29′ 18″	38° 50′ 23″	28.6	Evergreen	Loam	0.875	0.896	0.933	0.931
3	−120° 24′ 22″	38° 46′ 46″	32.5	Woodland	Sandy loam	0.815	0.838	0.861	0.864
4	−120° 23′ 34″	38° 46′ 37″	27.4	Woodland	Sandy loam	0.987	1.016	1.040	1.047
5	−120° 23′ 23″	38° 46′ 33″	24.1	Woodland	Sandy loam	0.997	1.026	1.050	1.058
6	−120° 22′ 53″	38° 46′ 23″	36.1	Woodland	Sandy loam	0.988	1.012	1.040	1.040
7	−120° 21′ 34″	38° 46′ 05″	31.1	Woodland	Sandy loam	0.856	0.881	0.905	0.908
8	−120° 20′ 28″	38° 46′ 04″	29.6	Woodland	Sandy loam	0.939	0.965	0.994	0.992
9	−120° 16′ 33″	38° 46′ 58″	36.6	Woodland	Sandy loam	0.988	1.014	1.025	1.040
10	−120° 16′ 47″	38° 46′ 20″	34.9	Woodland	Sandy loam	0.751	0.775	0.802	0.796

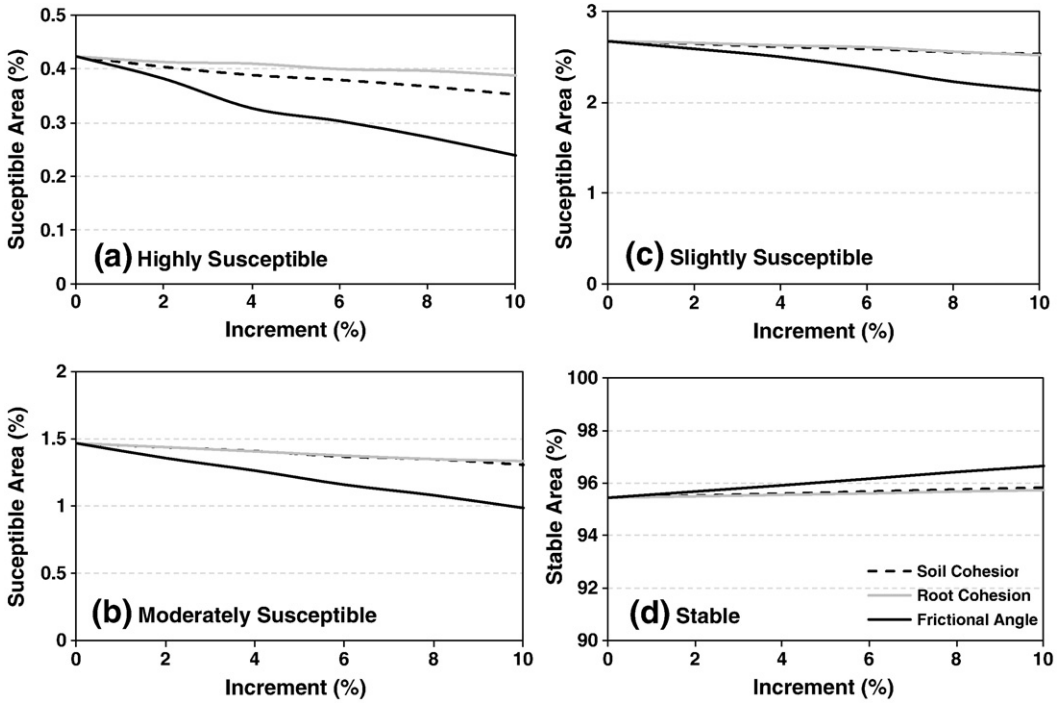

Fig. 10. Impact of soil cohesion, root cohesion and angle of internal friction on slope instability.

Acknowledgements

We acknowledge NASA's research funding through Earth System Science Fellowship, Grant No: NNG05GP66H, for this research. We would also like to thank Dr. M.E. Reid for providing information about Cleveland Corral Landslide area and in-situ groundwater measurements. We are indebted to three reviewers whose extensive comments greatly improved the manuscript.

References

Abdallah, C., Chowrowicz, J., Bouheir, R., & Dhont, D. (2007). Comparative use of processed satellite images in remote sensing of mass movements: Lebanon as a case study. *International Journal of Remote Sensing*, *28*(19), 4409−4427.

Acharya, G., De Smedt, F., & Long, N. T. (2006). Assessing landslide hazard in GIS: A case study from Rasuwa, Nepal. *Bulletin of Engineering Geology and the Environment*, *65*(1), 99−107.

Brarddinoni, F., Slaymaker, O., & Hassan, M. A. (2003). Landslide inventory in rugged forested watershed: A comparison between air-photo and field survey data. *Geomorphology*, *54*, 179−196.

Brooks, R. H., & Corey, A. T. (1988). Hydraulic properties of porous media. Hydrol. Pap. Colorado State University, 3.

Canuti, P., Casagli, N., Ermini, L., Fanti, R., & Farina, P. (2004). Landslide activity as a geoindicator in Italy: Significance and new perspectives from remote sensing. *Environmental Geology*, *45*(7), 907−919.

Carrara, A., Cadinali, M., Detti, R., Guzzetti, F., Pasqui, F., & Reichenbach, P. (1991). GIS techniques and statistical models in evaluating landslide hazard. *Earth Surface Processes and Landforms*, *16*, 427−445.

Chauhan, N. S., Miler, S., & Aradny, P. (2003). Spaceborn soil moisture estimation at high resolution: A microwave-optical/IR synergistic approach. *International Journal of Remote Sensing*, *24*(22), 4599−4622.

Cheng, K. S., Wei, C., & Chang, S. C. (2004). Locating landslides using multi-temporal satellite images. *Advances in Space Research*, *33*, 296−301.

Cherkauer, K. A., & Lettenmaier, D. P. (1999). Hydrologic effect of frozen soils in the upper Mississippi river basin. *Journal of Geophysical Research-Atmospheres*, *104* (D16), 19599−19610.

Choi, M., & Jacobs, J. M. (2008). Temporal variability corrections for Advanced Microwave Scanning Radiometer E (AMSR-E) surface soil moisture: Case study in Little River Region, Georgia, U.S.. *Sensors*, *8*, 2617−2627.

Choi, M., Jacobs, J. M., & Bosch, D. D. (2008). Remote sensing observatory validation of surface soil moisture using Advanced Microwave Scanning Radiometer E, Common Land Model, and ground based data: Case study in SMEX03 Little River Region, Georgia, U.S.. *Water Resources Research*, *44*, W08421. doi:10.1029/2006WR005578.

Clapp, R. B., & Hornberger, G. M. (1978). Empirical equations for some soil hydrologic properties. *Water Resources Research*, *14*(4), 601−604.

Dengzhong, Z, & Wanchang, Z. (2005). Rainfall-runoff simulation using the VIC-3L model over the Heihe River mountainous basin, China. IEEE, 0-7803-9050-4/05, 4391-4394.

Deoja, B. B., Dhital, M., Thapa, B., & Wagner, A. (1991). Mountain risk engineering handbook. Kathmandu: International Centre for Integrated Mountain Development (ICIMOD).

De Vleeschauwer, C., & De Smedt, F. (2002). Modeling slope stability using GIS on a regional scale. *Proceedings of the first Geological Belgica International Meeting, Leuven, 11–15 September 2002. Aardkundige Mededelingen*, *12*. (pp. 253−256).
Dingman, S. L. (2002). *Physical hydrology* (pp. 646). New Jersey: Prentice Hall, Upper Saddle River.
Doubkova, M., Sabel, D., Pathe, C., Hasenauer, S., Bartsch, A., & Wagner, W. (2008). High resolution soil moisture from radar instruments: Study area of northeast Austria and southeast Czech Republic. HydroPredict-Prague, Czech Republic; Bruthans-Kovar-Hrkal (eds), 89–92.
Drusch, M. (2007). Initializing numerical weather prediction models with satellite-derived surface soil moisture: Data assimilation experiments with ECMWF's Integrated Forecast System and the TMI soil moisture data set. *Journal of Geophysical Research*, *112*, D03102. doi:10.1029/2006JD007478.
Francini, M., & Pacciani, M. (1991). Comparative analysis of several conceptual rainfall-runoff models. *Journal of Hydrology*, *122*, 161−219.
Gao, H., Wood, E. F., Jackson, T. J., Drusch, M., & Bindlish, R. (2006). Using TRMM/TMI to retrieve surface soil moisture over the southern United States from 1998 to 2002. *Journal of Hydrometeorology*, *7*, 23−38.
Gorsevski, P. V., Gessler, P. E., & Jankowski, P. (2003). Integrating a fuzzy k-means classification and a Bayesian approach for spatial prediction of landslide hazard. *Journal of Geographical Systems*, *5*(3), 223−251.
Gruhier, C., de Rosnay, P., Hasenauer, S., Holmes, T., de Jeu, R., Kerr, Y., et al. (2010). Soil moisture active and passive microwave products: intercomparison and evaluation over a Sahelian site. *Hydrology and Earth System Sciences*, *14*, 141−156.
Gruhier, C., de Rosnay, P., Kerr, Y., Mougin, E., Ceschia, E., & Calvet, J. C. (2008). Evaluation of AMSR-E soil moisture product based on ground measurements over temperate and semi-arid regions. *Geophysical Research Letters*, *35*, L10405. doi:10.1029/2008GL033330.
Guzzetti, F., Carrara, A., Cardinali, M., & Reichenbach, P. (1999). Landslide hazard evaluation: A review of current techniques and their application in a multi-scale study, Central Italy. *Geomorphology*, *31*(1–4), 181−216.
Hallikainen, M. T., Ulaby, F. T., Dobson, M. C., El-rayes, M. A., & Wu, L. (1985). Microwave dielectric behavior of wet soil − part I: Empirical models and experimental observations. *IEEE Transactions on Geoscience and Remote Sensing*, *GE-23*(1), 25−34.
Hemakumara, M., Kalma, J., Walker, J., & Willgoose, G. (2004). Downscaling of low resolution passive microwave soil moisture observations. In A. J. Teuling, H. Leijnse, P. A. Troch, J. Sheffield, & E. F. Wood (Eds.), *Proceedings of the 2nd International CAHMDA Workshop on: The Terrestrial Water Cycle: Modeling and Data Assimilation Across Catchment Scales* (pp. 25−27). Princeton, NJ, October.
Hervas, J., Barredo, J. I., Rosin, P. L., Pasuto, A., Mantovani, F., & Silvano, S. (2003). Monitoring landslides from optical remotely sensed imagery: the case history of Tessina landslide, Italy. *Geomorphology*, *54*, 63−75.
Hong, Y., Adler, R., & Huffman, G. (2007). Use of satellite remote sensing data in the mapping of global landslide susceptibility. *Natural Hazards*, *43*, 245−256.
Hossain, A. K. M. A., & Easson, G. (2008). Evaluating the potential of VI-LST Triangle model for quantitative estimation of soil moisture using optical imagery. *IEEE International Geosciences and Remote Sensing Symposium (IGARSS), Boston, USA* (pp. III-47-50).978-1-4244-2808-3.
Huang, M., & Liang, X. (2006). On the assessment of the impact of reducing parameters and identification of parameter uncertainties for a hydrologic model with applications to ungauged basins. *Journal of Hydrology*, *320*, 37−61.
Jackson, T. J., Bindlish, R., Gasiewski, A. J., Stankov, B., Njoku, E. G., Bosch, D., et al. (2005). Polarimetric scanning radiometer C- and X-band microwave observations during SMEX03. *IEEE Transactions on Geoscience and Remote Sensing*, *43*(11), 2418−2430.
Jackson, T. J., Moran, M. S., & O'Neill, P. E. (2008). Introduction to soil moisture experiments 2004 (SMEX04) special issue. *Remote Sensing of Environment*, *112*, 301−303.
Jones, L. A., Kimball, J. S., Podest, E., McDonald, K. C., Chan, S. K., & Njoku, E. G. (2009). A method for deriving land surface moisture, vegetation, and open water fraction from AMSRE. *IEEE Int. Geosci. Rem. Sens. Symp. IGARSS '09, July 13–17, Cape Town, South Africa*.
Kaab, A. (2005). Combination of SRTM3 and repeat ASTER data for deriving alpine glacier flow velocities in the Bhutan Himalaya. *Remote Sensing of Environment*, *94*, 463−474.
Lacava, T., Greco, M., Di Leo, E. V., Martino, G., Pergola, N., Sannazzaro, F., et al. (2005). Monitoring soil wetness variations by means of satellite passive microwave observations: the HYDROPTIMET study cases. *Natural Hazards and Earth System Sciences*, *5*, 583−592.
Lakhankar, T., Krakauer, N., & Khanbilvardi, R. (2009). Application of microwave remote sensing of soil moisture for agricultural applications. *International Journal of Terraspace Science and Engineering*, *2*(1), 81−91.
Li, L., Njoku, E. G., Chang, P. S., & Germain, K. S. (2004). A preliminary survey of radio-frequency interference over the U.S. in Aqua AMSR-E data. *IEEE Transactions on Geoscience and Remote Sensing*, *42*(2), 380−390.
Liang, X., Lettenmaier, D. P., Wood, E. F., & Burges, S. J. (1994). A simple hydrologically based model of land surface water and energy fluxes for GSMs. *Journal of Geophysical Research*, *99*(D7), 14415−14428.
Liang, X., Wood, E. F., & Lettenmaier, D. P. (1996). Surface soil moisture parameterization of the VIC-2L model: Evaluation and modifications. *Global and Planetary Change*, *13*, 195−206.
Liang, X., Wood, E. F., & Lettenmaier, D. P. (1999). Modeling ground heat flux in land surface parameterization schemes. *Journal of Geophysical Research*, *104*(D8), 9581−9600.
Liang, X., & Xie, Z. (2003). Important factors in land–atmosphere interactions: Surface runoff generations and interactions between surface and groundwater. *Global and Planetary Change*, *38*, 101−114.
Lohmann, D., Raschike, E., Nijssen, P., & Lettenmaier, D. P. (1998). Regional scale hydrology: I. Formulation of the VIC-2L model coupled to a routing model. *Hydrological Sciences Journal*, *43*(1), 131−141.
Luo, Y., Trishchenko, A. P., & Khlopenkov, K. V. (2008). Developing clear-sky, cloud shadow mask for producing clear-sky composites at 250-meter spatial resolution for the seven MODIS land bands over Canada and North America. *Remote Sensing of Environment*, *112*, 4167−4185.
Mantovani, F., Soeters, R., & van Westen, C. J. (1996). Remote sensing techniques for landslide studies and hazard zonation in Europe. *Geomorphology*, *15*, 213−225.
Maurer, E. P., Wood, A. W., Adam, J. C., Lettenmaier, D. P., & Nijssen, B. (2002). A long-term hydrologically based dataset of land surface fluxes and states for the conterminous United States. *Journal of Climate*, *15*, 3237−3251.
McCabe, M. F., Gao, H., & Wood, E. F. (2005). Evaluation of AMSR-E derived soil moisture retrievals using ground-based and PSR airborne data during SMEX02. *Journal of Hydrometeorology − Special Edition*, *6*, 864−877.
Miller, D. A., & White, R. A. (1998). A conterminous United States multi-layer soil characteristics data set for regional climate and hydrology modeling.*Earth Interactions*, *2* [Available on-line at http://www.EarthInteractions.org].
Mitchell, K. E., Lohman, D., Houser, P. R., Wood, E. F., Schaake, J. C., Robock, A., et al. (2004). The multi-institution North American Land Data Assimilation System (NLDAS): Utilizing multiple GCIP products and parameters in a continental distributed hydrological modeling system. *Journal of Geophysical Research*, *109*, Do7S90. doi:10.1029/2003JD003823.
Montgomery, D. R., & Dietrich, W. E. (1994). A physically based model for the topographic control on shallow landsliding. *Water Resources Research*, *30*(4), 1153−1171.
Moran, M. S., Peter-Lidard, C. D., Watts, J. M., & McElroy, S. (2004). Estimating soil moisture at the watershed scale with satellite-based radar and land surface models. *Canadian Journal of Remote Sensing*, *30*(5), 805−826.
Nichol, J., & Wong, M. S. (2005). Satellite remote sensing for detailed landslide inventories using change detection and image fusion. *International Journal of Remote Sensing*, *26*(9), 1913−1926.
Nijssen, B., Lettenmaier, D. P., Liang, X., Wetzel, S. W., & Wood, E. F. (1997). Streamflow simulation for continental-scale river basins. *Water Resources Research*, *33*(4), 711−724.
Nijssen, B., Schnur, R., & Lettenmaier, D. P. (2001). Global retrospective estimation of soil moisture using the variable infiltration capacity land surface model, 1980–93. *Journal of Climate*, *14*, 1790−1808.
Njoku, E. G., & Chan, S. K. (2006). Vegetation and surface roughness effects on AMSR-E land observations. *Remote Sensing of Environment*, *100*, 190−199.
Njoku, E. G., Jackson, T. J., & Koike T. (2000). AMSR-E Science Data Validation Plan (pp. 76), version 2, 7/00.
Njoku, E. G., Jackson, T. J., Lakshmi, V., Chan, T. K., & Nghiem, S. V. (2003). Soil moisture retrieval from AMSR-E. *IEEE Transactions on Geoscience and Remote Sensing*, *412*(2), 215−229.
Oka, N. (1998). Application of photogrammetry to the field observation of failed slopes. *Engineering Geology*, *50*, 85−100.
Ostir, K., Veljanovski, T., Podobanikar, T., & Stancic, Z. (2003). Application of satellite remote sensing in natural hazard management: The Mount Mangart landslide case study. *International Journal of Remote Sensing*, *24*(20), 3983−4002.
Pack, R. T., Tarboton, D. G., & Goodwin, C. N. (1998). The SINMAP approach to terrain stability mapping. In D. P. Moore, & O. Hungr (Eds.), *Proceedings − International Congress of the International Association for Engineering Geology and the Environment 8, 2* (pp. 1157−1165). Rotterdam, Netherlands: A.A. Balkema.
Parada, L. M., & Liang, X. (2004). Optimal multiscale Kalman filter for assimilation for near-surface soil moisture into land surface models. *Journal of Geophysical Research*, *109*, D24109. doi:10.1029/2004JD004745.
Pelletier, J. D., Malamud, B. D., Blodgett, T., & Turcotte, D. L. (1997). Scale-invariance of soil moisture variability and its implications for the frequency-size distribution of landslides. *Engineering Geology*, *48*(3–4), 255−268.
Pradhan, B., Singh, R. P., & Buchroithner, M. F. (2006). Estimation of stress and its use in evaluation of landslide prone regions using remote sensing data. *Advances in Space Research*, *37*, 698−709.
Rawls, W. J., Brakensiek, D. L., & Saxton, K. E. (1982). Estimation of soil water properties. *Transactions of the American Society of Agricultural Engineers*, *25(5)*, 1316−1320.
Ray, R. L. (2004). Slope Stability Analysis using GIS on a Regional Scale: a case study from Dhading, Nepal. MSc. thesis in Physical Land Resources, Vrije Universiteit Brussel, 98 pp.
Ray, R. L., & Jacobs, J. M. (2007). Relationships among remotely sensed soil moisture, precipitation and landslide events. *Natural Hazards*, *43*(2), 211−222.
Ray, R. L., Jacobs, J. M., & de Alba, P. (2010). Impact of vadose zone soil moisture and groundwater in slope instability. *Journal of Geotechnical and Geoenvironmental Engineering*. doi:10.1061/(ASCE)GT.1943-5606.0000357.
Reichle, R. H., Koster, R. D., Dong, J., & Berg, A. A. (2004). Global soil moisture from satellite observations, land surface models, and ground data: Implications for data assimilation. *Journal of Hydrometeorology*, *5*, 430−442.
Reid, M. E. (2007). Personal communication. USGS. http://www.landslides.usgs.gov/monitoring/hwy50/
Reid, M. E., Brien, D. L., LaHusen, R. G., Roering, J. J., de la Fuente, J., & Ellen, S. D. (2003). Debris-flow initiation from large, slow-moving landslides. In Rickenmann, & Chen (Eds.), *Debris-flow hazards mitigation: Mechanics, prediction, and assessment*. Rotterdam: Millpress90 77017 78X.
Rosso, R., Rulli, M. C., & Vannucchi, G. (2006). A physically based model for the hydrologic control on shallow landsliding. *Water Resources Research*, *42*, W06410. doi:10.1029/2005WR004369.
Saha, A. K., Gupta, R. P., & Arora, M. K. (2002). GIS-based landslide hazard zonation in the Bhagirathi (Ganga) Valley, Himalayas. *International Journal of Remote Sensing*, *23*(2), 357−369.
Sahoo, A. K., Houser, P. R., Ferguson, C., Wood, E. F., Dirmeyer, P. A., & Kafatos, M. (2008). Evaluation of AMSR-E soil moisture results using the in-situ data over the Little River experimental Watershed, Georgia. *Remote Sensing of Environment*, *112*, 3142−3152.

Sarkar, S., & Kanungo, D. P. (2004). An integrated approach for landslide susceptibility mapping using remote sensing and GIS. *Photogrammetric Engineering and Remote Sensing*, *70*(5), 617−625.

Schmugge, T. J., Kustas, W. P., Ritchie, J., Jackson, T. J., & Rango, A. (2002). Remote sensing in hydrology. *Advances in Water Resources*, *25*, 1367−1385.

Sidle, R. C., & Ochiai, H. (2006). *Landslides: Processes, prediction, and land use. Water Resources Monograph*, *18*. (pp. 312) : American Geophysical Union.

Singhroy, V., & Molch, K. (2004). Characterizing and monitoring rockslides from SAR techniques. *Advances in Space Research*, *33*, 290−295.

Skempton, A. W., & DeLory, F. A. (1957). Stability of natural slopes in London clay. *Proceedings 4th International Conference on Soil Mechanics and Foundation Engineering London*, *2*. (pp. 378−381).

Soil Survey Staff, Natural Resources Conservation Service, United States Department of Agriculture. U.S. General Soil Map (STATSGO) for CA, Jan 4, 2008 http://www.soildatamart.nrcs.usda.gov

Spittler, T. E., & Wagner, D. L. (1998). Geology and slope stability along Highway 50. *California Geology*, *51*(3), 3−14.

van Westen, C. J. (1994). GIS in landslide hazard zonation: A review, with examples from the Andes of Colombia. In M. F. Price, & D. I. Heywood (Eds.), *Mountain environments and geographic information systems* (pp. 135−165). : Taylor and Francis Publishers.

van Westen, C. J., & Getahun, F. L. (2003). Analyzing the evolution of the Tessina landslide using aerial photographs and digital elevation models. *Geomorphology*, *54*, 77−89.

van Westen, C. J., & Trelirn, T. J. (1996). An approach towards deterministic landslide hazard analysis in GIS: A case study from Manizales (Colombia). *Earth Surface Processes and Landforms*, *21*, 853−868.

Varnes, D. J. (1984). Landslide Hazard Zonation: A Review of Principles and Practice. Commission on the Landslides of the IAEG, UNESCO, Natural Hazard 3:66 pp.

Vivoni, E. R., Gabremichael, M., Watts, C. J., Bindlish, R., & Jackson, T. J. (2008). Comparison of ground-based and remotely-sensed surface soil moisture estimates over complex terrain during SMEX04. *Remote Sensing of Environment*, *112*, 314−325.

Wagner, W., Pathe, C., Doubkova, M., Sabel, D., Bartsch, A., Hasenauer, S., et al. (2008). Temporal stability of soil moisture and radar backscatter observed by the Advanced Synthetic Aperture Radar (ASAR). *Sensors*, *8*, 1174−1197.

Walker, J. P., Houser, P. R., & Willgoose, G. R. (2004). Active microwave remote sensing for soil moisture measurement: A field evaluation using ERS-2. *Hydrological Processes*, *18*, 1975−1997.

Wang, L., Wen, J., Zhang, T., Zhao, Y., Tian, H., Shi, X., et al. (2009). Surface soil moisture estimates from AMSR-E observations over an arid area, Northwest China. *Hydrology and Earth System Sciences Discussion*, *6*, 1056−1087.

Wood, E. F., Lettenmaier, D. P., & Zartarain, V. G. (1992). A land-surface hydrology parameterization with subgrid variability for general circulation models. *Journal of Geophysical Research*, *97*(D3), 2717−2728.

Yu, G., Di, L., & Yang, W. (2008). Downscaling of global soil moisture using auxiliary data. IEEE, 978-1-4244-2808-3/08, I-304-307.

Yuan, F., Xie, Z., Liu, Q., Yang, H., Su, F., Liang, X., et al. (2004). An application of the VIC-3L land surface model and remote sensing data simulating streamflow for theHanjiang River basin. *Canadian Journal of Remote Sensing*, *30*(5), 680−690.

Yulin, C., Zhifeng, G., & Li, Y. (2008). A macro hydrologic model simulation based on remote sensing data. 2008 International Workshop on Earth Observation and Remote sensing Applications, IEEE 1-4244-2394-1/08. 4 pp.

Zhou, S. Q., Liang, X., Chen, J., & Gong, P. (2004). An assessment of the VIC-3L hydrological model for the Yangtze River basin based on remote sensing: A case study of the Baohe River basin. *Canadian Journal of Remote Sensing*, *30*(5), 840−853.

Zomer, R., Ustin, S., & Ives, J. (2002). Using satellite remote sensing for DEM extraction in complex mountainous terrains: Landscape analysis of the Makalu Barun National Park of eastern Nepal. *International Journal of Remote Sensing*, *23*(1), 125−143.